Available online at www.sciencedirect.com
ScienceDirect
Polymer 48 (2007) 6913–6922
polymer
www.elsevier.com/locate/polymer

Effects of parameters on nanofiber diameter determined from electrospinning model

C.J. Thompson [a], G.G. Chase [a,*], A.L. Yarin [b], D.H. Reneker [c]

[a] Department of Chemical and Biomolecular Engineering, The University of Akron, Akron, OH 44325-3906, United States
[b] Department of Mechanical and Industrial Engineering, The University of Illinois at Chicago, Chicago, IL 60607-7022, United States
[c] Department of Polymer Science, The University of Akron, Akron, OH 44325-3906, United States

Received 26 June 2007; received in revised form 8 September 2007; accepted 10 September 2007
Available online 15 September 2007

Abstract

In this paper the effects of 13 material and operating parameters on electrospun fiber diameters are determined by varying the parameter values in an electrospinning theoretical model. The complexity of the electrospinning process makes empirical determination of the effects of parameters very difficult. The results show that the five parameters (volumetric charge density, distance from nozzle to collector, initial jet/orifice radius, relaxation time, and viscosity) have the most significant effect on the jet radius. The other parameters (initial polymer concentration, solution density, electric potential, perturbation frequency, and solvent vapor pressure) have moderate effects on the jet radius. Parameters relative humidity, surface tension, and vapor diffusivity have minor effects on the jet radius. Knowing the relative effects of parameters on jet radius should be useful for process control and prediction of electrospun fiber production.

Keywords: Electrospinning; Nanofiber; Polymer jet

1. Introduction

Nanofibers produced by electrospinning are of industrial and scientific interest due to their long lengths, small diameters, and high surface area per unit volume. The process is complex with the resulting jet (fiber) diameter being influenced by numerous material, design, and operating parameters. A significant part of our information of the electrospinning process comes from empirical observations but the complexity of the process makes empirical determination of parameter effects very difficult if not impractical.

By using a suitable theoretical model of the electrospinning process the effects of parameters on the fiber diameter can be evaluated. The models should indicate which parameters have the greatest influence on the fiber diameters. Hence, these parameters are the ones to focus on in the empirical studies.

The objective of this work is to apply the only existing model of electrospinning [1,2], accounting for the large nonlinear perturbations, viscoelasticity, evaporation and solidification, to determine the effects of the parameters on the fiber diameter. The parameters are evaluated on a relative basis to determine a strong–moderate–minor rating for the influence of the parameters on the nanofiber diameter [3].

Several models of electrified and electrospinning jets have been developed. The usual intents of scientific models apply here, such as to help us to understand the process, control the process, or to improve upon process limitations. Some notable electrospinning characteristics include:

1. Volume production rates are relatively low. Ref. [4] reported production rates of about 2–5 kg of nanofiber per day at one facility, while in Ref. [5] it was shown that a 12-fold increase in the production rate is possible.
2. It is easier to form nonwoven mats than aligned fibers. Nevertheless, methods employing electrostatic lenses

* Corresponding author. Tel.: +1 330 972 7943.
E-mail address: gchase@uakron.edu (G.G. Chase).

0032-3861/$ - see front matter © 2007 Elsevier Ltd. All rights reserved.
doi:10.1016/j.polymer.2007.09.017

were proposed to manufacture oriented nanofiber arrays, crossbars and nanoropes [6–8].

3. Predictions of as-spun nanofiber diameter and/or diameter distribution are not reliable.
4. Difficulty in controlling nanofiber morphology: diameter uniformity, formation or absence of beads related to capillary instability.
5. Absence of detailed information on rheological behavior of semi-dilute and concentrated polymer solutions used in electrospinning, especially information on elongational behavior in extremely strong uniaxial elongational flows characteristic of electrospinning.
6. Process control is not as precise as desired, even though a model [1,2] has already been generalized for the case of multiple electrospun jets [9].

Nanofiber properties can vary dramatically given the many variables that may influence the process such as the polymer (type, molecular weight), solvent (types, vapor pressure, diffusivity in air), additives (surfactants, salts), polymer concentration, solution properties (rheological behavior, relaxation time, viscosity, surface tension, electric conductivity and dielectric permittivity), electric field (strength, geometry), solution feed rate, nozzle orifice diameter, distance from nozzle to collector, and ambient conditions (relative humidity, temperature, etc.).

Theoretical prediction and understanding of the parameter effects on jet radius and morphology could significantly reduce experimental time by identifying the most likely values that will yield specific qualities prior to production. For example, the physical control of nanofiber size remains a technological bottleneck. Empirical observations indicate that the smallest diameters occur at the lowest flow rates, but production rate and fiber size tend to vary with the solution concentration. Unfortunately, using the solution concentration as the control variable limits production to a narrow window of spinnable solution concentrations [10]. An accurate, predictive tool using a verifiable model that accounts for multiple factors would provide a means to run many different scenarios quickly without the cost and time of experimental trial-and-error.

Some of the models of electrified and electrospun jets reported in literature are listed in Table 1. Early observations of the electrospinning jets suggested that the jets splay, whereas material points move along straight secondary jets conically outflowing from the splaying point. Detailed video observations taken by a high-speed CCD camera and modeling in Ref. [1] showed that instead of splaying, an electrospun jet stays intact, while vigorously bending and stretching inside a conical envelope. Snapshots of an electrospun jet inside the envelope cone show a highly spiraling jet morphology. However, material points do not move along spirals but follow simpler paths spanning them, as modeling in Refs. [1,2] shows: a sketch is depicted in Fig. 1. The sketch in Fig. 1 shows 3D and top views of a typical snapshot of an electrospun jet and the path followed by a material point in time.

Table 1
Brief list of several models of electrified and electrospun jets and some of their key features

Reference	Features
[11]	Straight electrified jet, viscous Newtonian or shear-thinning power-law liquid
[12,13]	Linear stability analysis of small capillary and bending perturbations of electrified viscous Newtonian jet
[10]	Analysis of terminal diameter of a thinning electrified jet at the last stage of bending. The model does not account for viscoelasticity, solvent evaporation and polymer solidification. As a result, a disproportionately large role is attributed to surface tension
[14]	Straight electrified jet of viscoelastic liquid
[1,2,8,9]	Linear and nonlinear model (small and large perturbations) of the dynamics of single and multiple bending jets in electrospinning of polymer solutions. The model accounts for solution viscoelasticity, electric forces, solvent evaporation and solidification, surface tension and jet–jet interactions. It explains the physical mechanism of electrospinning and describes all the stages of the process

The intent of this paper is to determine how sensitive the electrospun nanofibers are to variations in parameters in a theoretical model. The only theoretical model available, which describes the whole electrospinning process accounting for the most important physical features is the one of Refs. [1,2]. Therefore, it is used in the present work. The model has been formulated using dimensionless representation. Therefore, in principle, the process analysis could be performed in the framework of the dimensional analysis, using variation of only the governing dimensionless groups, as it was done in Refs. [1,2,8,9,15]. However, an understanding of the dependence of the individual parameters can be better achieved by variation of the individual physical parameters, even though this way is more laborious. That is the reason why we chose to vary individual physical parameters instead of the dimensionless groups in the present work.

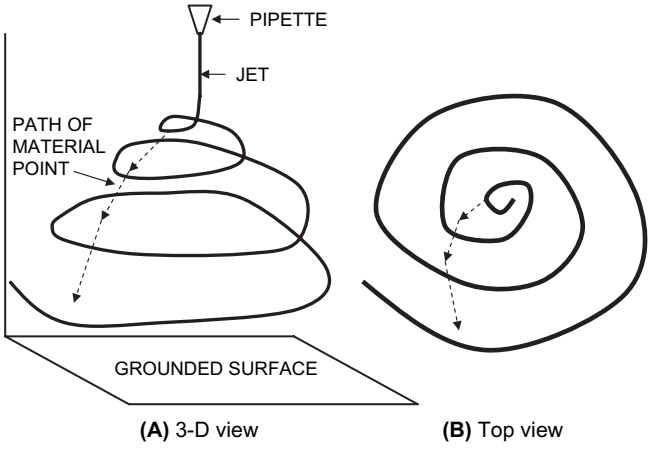

Fig. 1. 3D and top views of an instantaneous snapshot of an electrospinning spinline corresponding to a certain moment of time t_1 is shown by the solid curves. A path of a material point corresponding to different time moments ($t \geq t_1$) is shown by the dashed lines. It is emphasized that the jet snapshots at $t \geq t_1$ will still be comprised of similar spiral loops, albeit different from the shown one.

2. Analysis of parameter effects on nanofiber diameter

The analysis of the variable effects on the model predictions was performed for an aqueous polymer solution studied initially in Refs. [1,2]. The governing quasi-one-dimensional continuity, momentum and charge conservation equations read:

$$\begin{aligned} &\frac{\partial \lambda f}{\partial t} = -j_{\mathrm{ev}} \\ &\rho \frac{\partial \lambda f \mathbf{V}}{\partial t} = \tau \frac{\partial P}{\partial s} + \lambda |k| P n + \lambda |k| (\pi a \sigma - q_{\mathrm{el}}) n - \lambda e \frac{U_0}{h} \mathbf{k} \\ &e\lambda = e_0 \lambda_0 \end{aligned} \tag{1}$$

The equations are written using a Lagrangian parameter s "frozen" into the jet elements. In Eq. (1) λ is the geometrical stretching ratio, $f = \pi a^2$ is the cross-sectional area (a the cross-sectional radius), subscript zero denote the parameter values at time $t = 0$. Also, ρ is the liquid density, $\mathbf{V}$ its velocity vector, P the longitudinal force in the jet cross-section (of viscoelastic origin), U_0/h the outer electric field strength (U_0 the potential difference, h the inter-electrode distance; the outer field is assumed to be parallel to the unit vector $\mathbf{k}$), σ is the surface tension, k the local curvature of the jet axis, e the charge per unit jet length, q_{el} is the net Coulomb force acting on a jet element from all the other elements depending on e and the current overall configuration of the jet (calculated in detail in Refs. [1,2]), j_{ev} (>0) is the flux describing mass loss due to solvent evaporation from the jet surface (calculated in detail in Ref. [2]). The momentum equation in (1) neglects the shearing force in the jet cross-section, therefore there is no need for consideration of the moment-of-momentum equation and the theory is in fact momentless. The longitudinal force in the jet cross-section is determined by the normal stress in liquid (polymer solution acting there). It is related to the rheological constitutive equation (of the upper-convected Maxwell model, in the present case), as described in Refs. [1,2]. The rheological parameters depend on solvent concentration [2]. Therefore, Eq. (1) is also supplemented by the equations describing solvent evaporation from the jet [2].

The model predicts the evolution of the jet configuration driven by the bending instability, as well as the corresponding paths of individual material particles in the jet. In the present work we elucidate in detail the cross-sectional jet radius evolution and its final values in the as-spun nanofibers.

Table 2 lists the values of the 13 model input parameters used in the base case. The selected parameters encompass nearly all of the input parameters that can be used in the model, with the exception of temperature. However, temperature does factor indirectly into the calculations through changes in solution density, vapor diffusivity, viscosity, relaxation time, etc. To examine temperature effects, one must implement the dependences of all the other solution properties on temperature and (in the non-isothermal cases) include the thermal balance equation in consideration. Additionally, several other potential factors in the electrospinning process such as solution pH, charge polarity and pressure were not included in the model and as such not evaluated.

Table 2
Base case scenario model input parameters

Volumetric charge density (C/L)	1.0
Distance from nozzle to collector (cm)	20
Initial polymer concentration (wt%)	6
Density (gm/cm^3)	1.0
Electric potential (kV)	20
Relative humidity of solvent vapor in air (%)	1
Initial jet radius (cm)	0.015
Perturbation frequency (s^{-1})	10,000
Relaxation time (s)	0.01
Surface tension (dyn/cm)	70
Vapor diffusivity[a] (cm^2/s)	0.002
Solvent vapor pressure (mbar)	23.4
Initial elongational viscosity (P)	10,000

[a] The vapor diffusivity of 0.002 cm^2/s was used in the calculations but the correct diffusivity for water vapor is about 0.2 cm^2/s. This does not affect the parameter sensitivity results reported in this paper.

For each input parameter, ranges were selected based on literature data and step changes initially varied by a small amount around the base value to establish a general trend. In choosing reasonable step change values, some parameters have known limitations at the onset of electrospinning such as polymer concentration, numerically 0–100%, but actual electrospun solutions usually fall in the range of 5–30% depending on the polymer and solvent. Similarly the electric potential is limited by the dielectric breakdown in air at about 300 kV/m. Given a nozzle–collector separation distance of 20 cm, breakdown occurs at about 60 kV electric potential. For the parameters without known limitations, after the initial small changes around the base value, larger changes were made to ascertain the model solution limits and jet behavior under these conditions. To illustrate, surface tension value changes near the base had no affect on the jet evolution. Larger values, though unrealistic, were used which showed that surface tension had almost no affect. On the other hand, relatively small increases in volumetric charge density produced significant variations from the base, and additional increases caused divergence of the numerical solution.

While varying only a single parameter at a time is not practical in a physical sense, from a mathematical standpoint the particular contribution from a given parameter can be identified. For physical determination, given the interconnected nature of many of the parameters, a change in one could be offset by a change in another in order to obtain the desired solution quality (such as using two solvents). Moreover, some of the input parameters listed in Table 2 are not under full control in real experiments. For example, the model requests the initial cross-sectional radius of the jet as an input parameter only because it does not consider the jet formation at the tip of the Taylor cone, even though it can be done theoretically [2,16,17]. For such parameters, values roughly corresponding to the experimental observations are taken, however, effect of the other parameters (like of the applied voltage on the initial jet radius) are totally disregarded.

Once a model calculation was completed, and there were no numerical convergence problems, the final jet cross-sectional diameter was calculated for comparison with the base

case value. Fig. 2 shows the plot of the jet cross-sectional radius as a function of distance z from the grounded collector for the base case.

Some observations of the jet evolution predicted by the model for the base case scenario:

1. The jet cross-sectional radius starting at the nozzle (at $z = 20$ cm) toward the grounded surface (at $z = 0$) is observed to slightly increase as the jet approaches the onset point of the bending instability (at $z = 14$ cm) and then the jet radius decreases very rapidly over a distance of only a few centimeters where fully developed bending instability appears (Fig. 2). The increase in jet cross-sectional radius is attributed to a strong repulsion of the oncoming almost straight jet by the fully developed bending loops below carrying electric charge of the same sign.
2. In the vigorously bending loops the jet surface area increases dramatically as the jet undergoes huge stretching and elongation due to the electric forces. Such increase in the jet surface area dramatically accelerates solvent evaporation. The solvent concentration rapidly decreases in the bending loops, such that 90% has evaporated, only a few centimeters below the onset of the bending instability. Once the polymer concentration reaches about 90%, the jet continues to elongate, but at a much lower rate, as seen in the radius of the jet loops. The slower elongation rate is due to the increase in viscosity and elastic modulus of the solution at higher polymer concentrations. These results corroborate similar observations in Ref. [2].
3. The travel time of material elements in the jet from the nozzle to the collector is less than 0.02 s. The calculated volumetric flow rate and electrical current are 10.6 mL/h and 2.93 μA, and are similar to values experimentally observed in our laboratory.
4. In the basic case, the predicted final cross-sectional radius of the jet at the collector surface, at $z = 0$, is about 3×10^{-6} cm or equivalently about 600 nm in diameter. This size is within the ranges commonly observed in electrospinning. Of course smaller diameters of around 100 nm are often produced with some variation of the experimental process and operating parameters. The purpose of this paper is to determine which parameters have the greatest effect on the fiber diameter and to determine which parameters are the best for controlling the final cross-sectional radius of as-spun nanofibers.

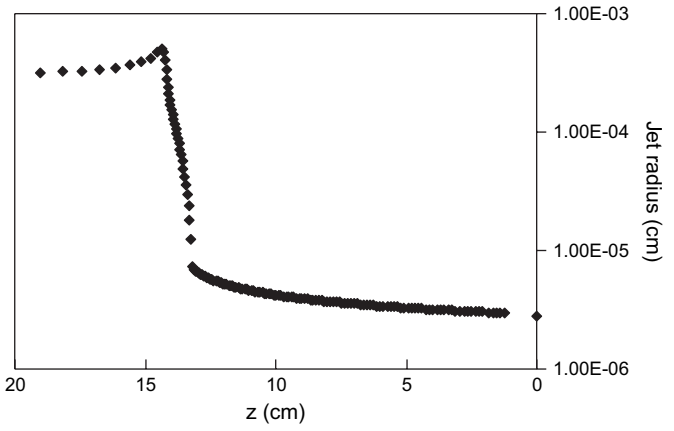

Fig. 2. The cross-sectional radius of the jet as a function of position (measured from the grounded surface). The nozzle holding the polymer drop is located at $z = 20$ cm. Each data point represents the radius value at one of the material elements in the polymer jet.

The effects of the parameter variations on the value of the jet cross-sectional radius are compared to the corresponding predictions for the base case described above. As an example, Fig. 3 illustrates the effect of the volumetric charge density on the jet radius, while all other parameter values are the same as for the base case. It should be noted that the model considers the volumetric charge density as an independent input parameter, not related to the applied voltage. In reality, however, the volumetric charge density would vary with the applied voltage. A detailed account for this inter-parameter effect is not practical at present, since it would require a detailed calculation of the solution flow and charging from a pump to the jet origin in additional to modeling the jet itself. Fig. 4 shows a plot of the final jet cross-sectional radius (rendered dimensionless by the final jet cross-sectional radius in the base case) versus the normalized volumetric charge density. The other parameters in this calculation were kept the same as in the base case.

A linear regression is applied to fit a straight line to the data in Fig. 4 and several other similar figures below. The slope of the fitted line is used for rating how strongly each parameter affects the final jet radius; the greater the magnitude of the line slope the stronger the effect on the final cross-sectional radius. Some of the parameters do not have a linear relationship and were fitted with a power-law expression to determine the range in the slopes. In these fitting lines the y-axis represents the normalized final cross-sectional radius of the jet and the x-axis is

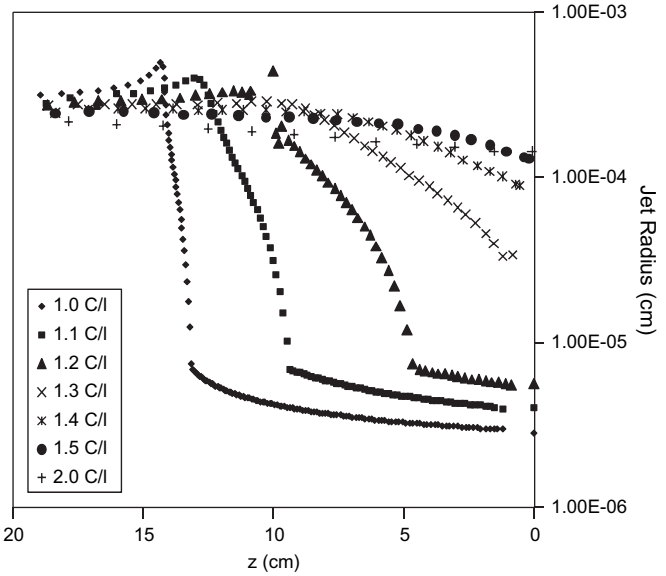

Fig. 3. Distributions of the jet radius along the jet versus z coordinate.

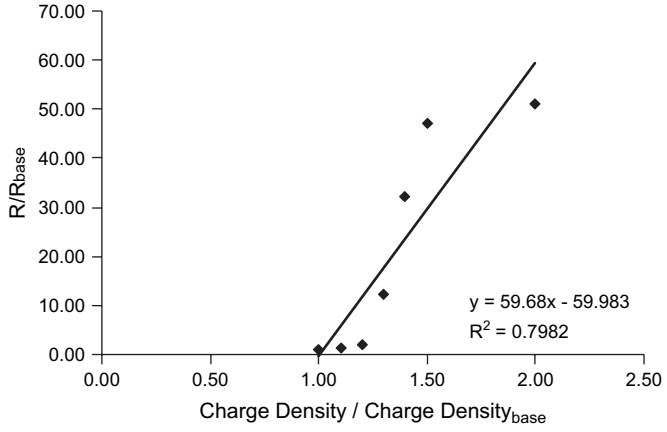

Fig. 4. Normalized final cross-sectional jet radius vs. normalized volumetric charge density.

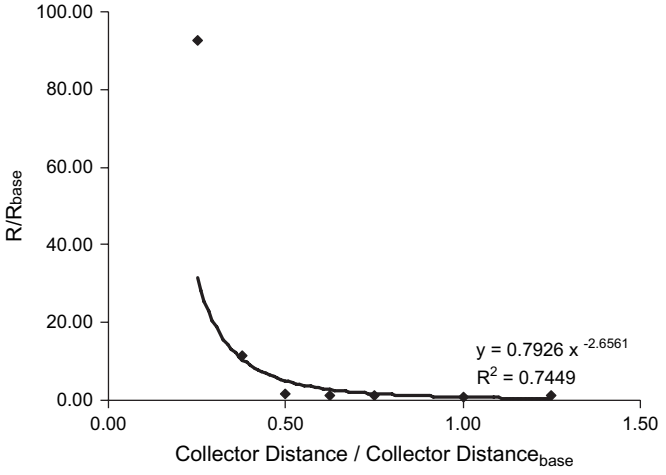

Fig. 5. Calculated final jet cross-sectional jet radius vs. normalized distance from nozzle to collector variation.

the normalized input parameter which has been varied in each case.

The model revealed a strong effect of the volumetric charge density on the fiber cross-sectional radius. Volumetric charge density is often determined during the electrospinning process by measuring the cumulative charge carried by the jet and dividing it by the cumulative volume of polymer solution delivered by the jet. The charge density depends on the solution's electrical properties (i.e. its electric conductivity related to the amount of dissolved electrolyte admixture and ion mobility, and dielectric permittivity of the solvent) and the applied electric potential. Theron et al. [18] provide experimental data on the effect of polymer type (PEO, polyvinyl alcohol, polyacrylic acid, polyurethane, and polycaprolactone), concentration, molecular weight, volumetric flow rate, solvent, applied voltage and nozzle-to-collector distance on the electric current and volumetric charge densities observed during electrospinning. Their results led to a conclusion that volumetric charge density depends on each of these parameters as a power-law relationship, except that the volumetric charge density depends on the nozzle-to-collector distance as an exponential relationship. Observed charge densities ranged from 0.001 to 10 C/L. The values of volumetric charge density used in the present model were in the range (0.2–3.0 C/L), i.e. were chosen based on those reported in literature, such as the work mentioned above and others, however, meaningful numerical solutions only converged for the values (1.0–2.0 C/L) reported in Figs. 3 and 4.

Figs. 5–16 show the normalized final cross-sectional radii versus the remaining governing parameters. The parameter value ranges were selected based on values reported in literature and on the stability of the model calculations. Linear regression provides an estimate of the slope even though in some cases the data show nonlinear behavior.

Ideally the normalized parameter values are evaluated at values greater and lesser than the base case, providing a range in the normalized horizontal axes above and below unity. In some cases the model calculations became unstable or were not reliable and those values are not reported. For example, in the cases of normalized (in regards of the base case) relative humidity values less than unity are not shown in the plot.

The results of these calculations are summarized in Table 3. Table 3 lists the regression coefficients for the curve fits as determined by MS Excel™. Some of the coefficients significantly deviate from unity indicating the fit is not very accurate, but visual inspection shows the slopes are reasonably well represented. In Figs. 5, 12, and 14 the data plots are highly nonlinear so power-law curves were fitted to the data.

The table shows a clearly defined split of the slopes into three groups, where the slopes indicate how strongly the parameters affect the final jet diameter. Based solely on the model calculations, the variables that most significantly affect the final jet radius are initial jet radius, charge density, nozzle-to-collector distance, initial elongational viscosity, and relaxation time. One parameter, the vapor diffusivity, could be placed either in the moderate or minor effect category; we have placed it in the minor category.

A brief comparison of the predicted results with reported literature data is given in the following:

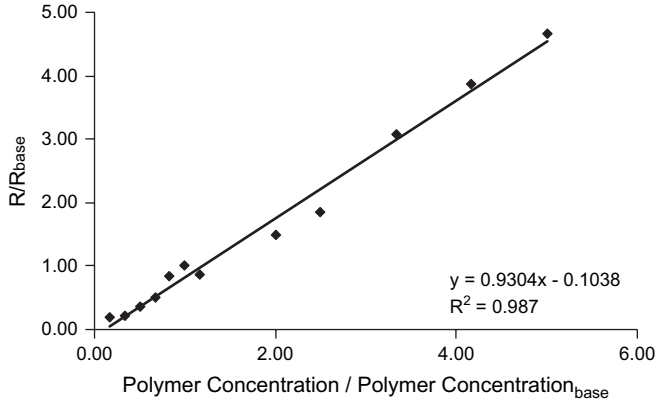

Fig. 6. Calculated final jet cross-sectional radius vs. normalized initial polymer concentration variation.

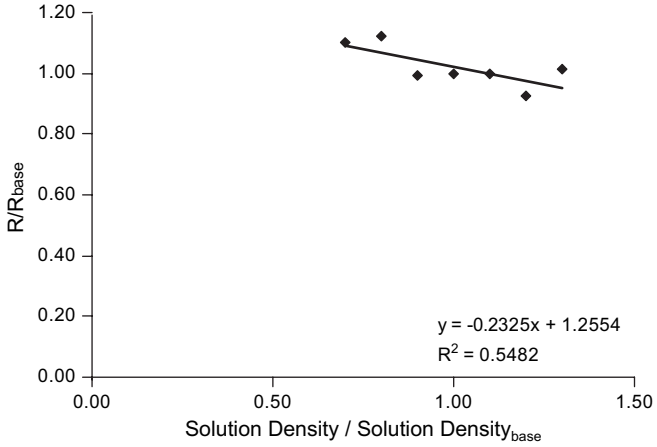

Fig. 7. Calculated final jet cross-sectional radius vs. normalized solution density variation.

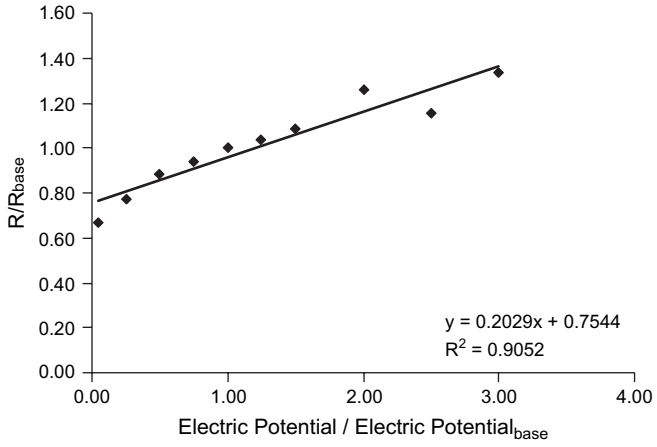

Fig. 8. Calculated final jet cross-sectional radius vs. normalized electrical potential variation.

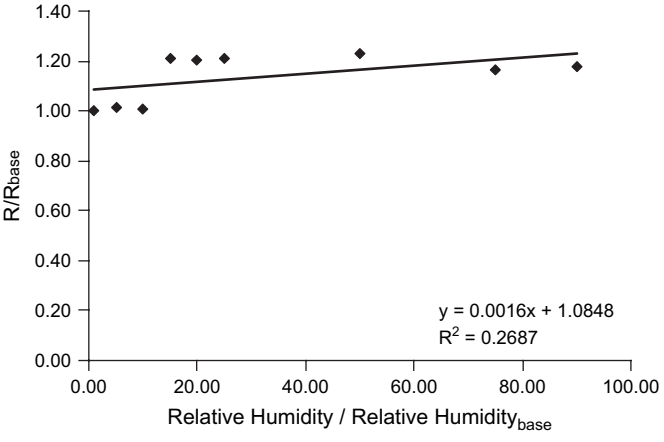

Fig. 9. Calculated final jet cross-sectional radius vs. normalized relative humidity variation.

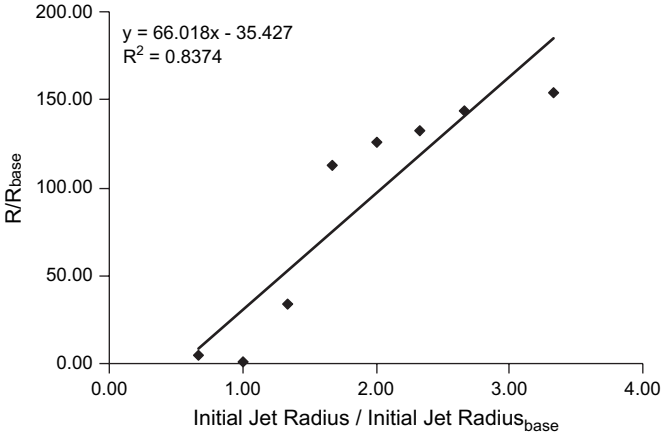

Fig. 10. Calculated final jet cross-sectional radius vs. normalized initial jet/orifice radius variation.

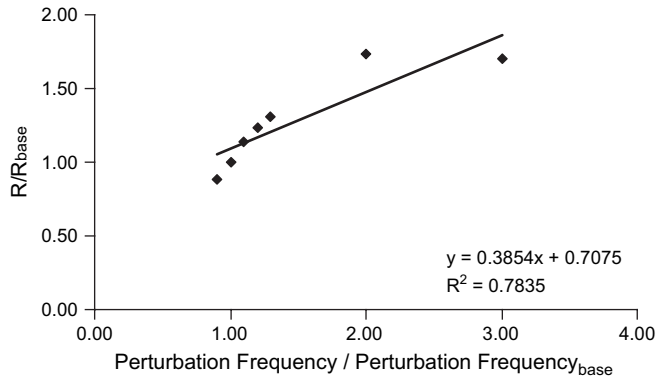

Fig. 11. Calculated final jet cross-sectional radius vs. normalized perturbation frequency variation.

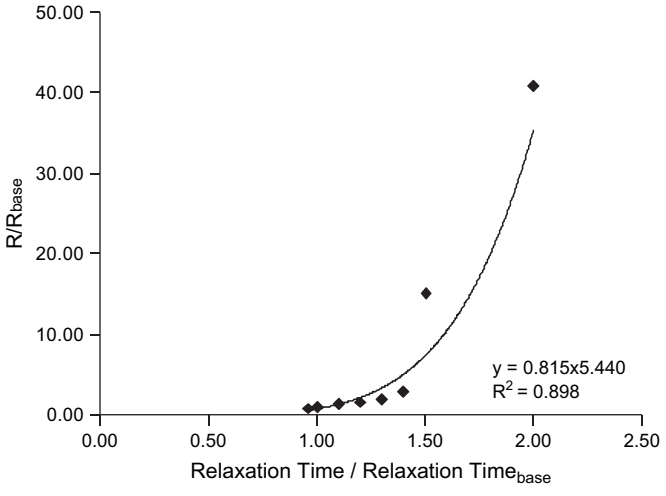

Fig. 12. Calculated final jet cross-sectional radius vs. normalized relaxation time variation.

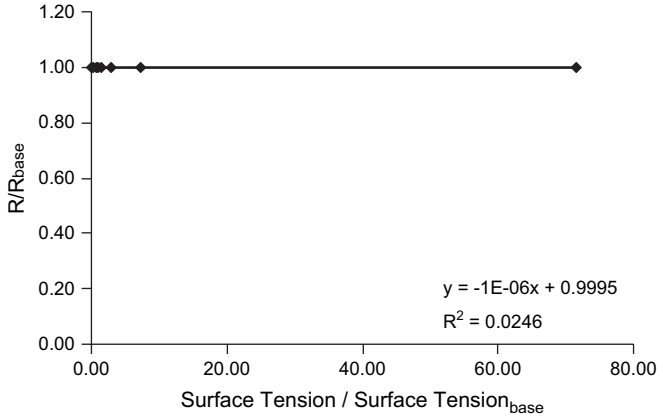

Fig. 13. Calculated final jet cross-sectional radius vs. normalized surface tension variation. MS Excel™ reports the R^2 value of 0.0246, but visual inspection of the linear fit and the data points shows the linear curve fits the data very well.

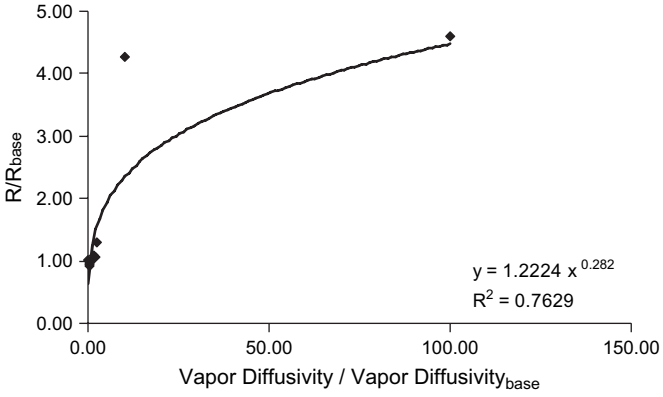

Fig. 14. Calculated final jet cross-sectional radius vs. normalized vapor diffusivity variation.

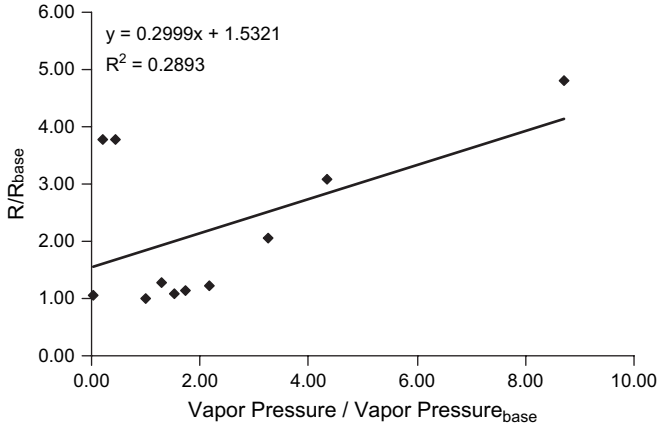

Fig. 15. Calculated final jet cross-sectional radius vs. normalized vapor pressure variation.

1. No papers report on the effect of initial jet radius on the final jet radius. The initial jet radius is related to the orifice size of the pipette supplying the polymer solution to the droplet shaped as the Taylor cone. Only a single paper [19] reported on the effect of orifice size on the resulting fiber diameter for electrospun poly(lactide-*co*-glycolide). Three orifices ranging from 0.029 to 0.059 cm were used to determine their effect on fiber diameter, while all other variables remained constant among each test. The results displayed average fiber diameters of 250, 150 and 125 nm for orifices of radii 0.059, 0.042 and 0.029 cm, respectively. This trend seems to match the model results with regard to increasing final fiber radius corresponding to the initial jet radius. It is emphasized that the initial jet diameter at the tip of the Taylor cone is significantly affected by the applied voltage. Therefore, it cannot be considered as a fully independent parameter when the applied voltage changes.
2. Ref. [20] observed for PEO/water solutions and ref. [21] observed for PHBV/chloroform solutions that polymer solution flow rate and volumetric charge density interrelation affects fiber morphology (smooth fibers versus fibers with beads). Increasing flow rate tends to increase fiber

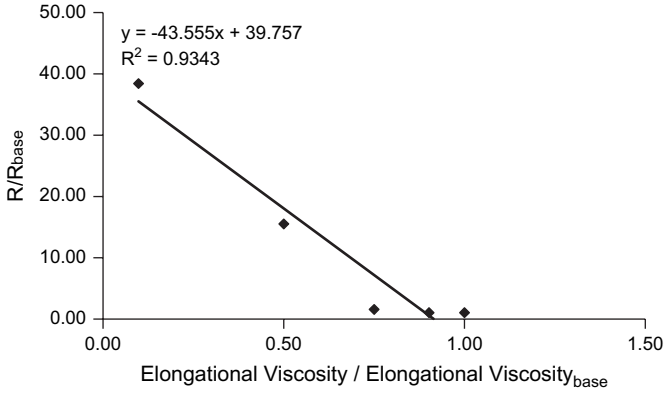

Fig. 16. Calculated final jet cross-sectional radius vs. normalized initial elongational viscosity variation.

Table 3
Summary of dependence of the final cross-sectional jet radius on input parameters

Parameter	Regression	Slope	R^2
Parameters with strong effect			
Initial jet radius	Linear	66	0.837
Volumetric charge density	Linear	60	0.798
Distance from nozzle to collector	Power-law	−2 to −21	0.745
Initial elongational viscosity	Linear	−44	0.934
Relaxation time	Power-law	4.4–96	0.898
Parameters with moderate effect			
Initial polymer concentration	Linear	0.93	0.987
Perturbation frequency	Linear	0.39	0.783
Solvent vapor Pressure	Linear	0.30	0.289
Solution density	Linear	−0.23	0.548
Electric potential	Linear	0.20	0.905
Parameters with minor effect			
Vapor diffusivity	Power-law	0.013–0.34	0.763
Relative humidity	Linear	0.0016	0.268
Surface tension	Linear	-1×10^{-6}	0.0246[a]

[a] Visual inspection of the curve fit of the data in Fig. 13 one would expect R^2 to be close to unity, but the calculated value reported by MS Excel™ is 0.0246. This may be a result of the linear curve having a nearly zero slope.

diameter and bead diameter. Other sources [22–28] reported similar observations as those mentioned in this item with regards to conductivity, flow rate and their relation to morphology and diameter. Literature sources report somewhat conflicting results with increases and decreases in jet radius with increasing volumetric charge density; however, this may be explained by competition between solution supply and demand via the shape of the droplet from which the jet emanates. Also, the volumetric charge density seems to play a significant role in the morphology of the fibers with the formation of beads for lower charge density solutions. Such solutions do not experience sufficient stretching by the electric force and do not build up a sufficient elongational viscosity. As a result, they can undergo capillary instability and develop beads [2]. The current modeling does not treat such cases. It is emphasized that volumetric charge density also cannot be considered as a fully independent parameter as the applied voltage varies.

3. Several literature sources [20,21,26–30] report separation distances between the nozzle and collector ranging from 7 to 50 cm in their experimental setups but not all sources report on effects of separation distance on final cross-sectional fiber diameter. For polystyrene solutions (using 18 different solvents), for collection distances at 7, 10 and 15 cm while maintaining everything else constant, Ref. [26] reports a decrease in fiber diameter with increase in collector distance when smooth fibers were produced. To the contrary, with beaded fibers present, the beads tended to grow larger as distance increased (probably because the capillary instability has more time to develop). Ref. [31] observed Nylon-6 fiber diameters decrease from 230 to 140 nm with gap distance changing from 4 to 18 cm, holding other parameters constant.
4. The initial elongational viscosity affects the model calculation on a similar scale, but opposite fashion to the relaxation time. Most viscosity values measured and reported are zero-shear values. The experimental data show a strong dependence on viscosity for fiber morphology [20,29]. Nearly every referenced work concluded that increasing zero-shear viscosity, whether by a higher MW polymer or higher concentration, will increase the resulting fiber radius, except when the nozzle becomes partially plugged or flow is somehow decreased such that a fully-supplied droplet is not available to the process. The initial elongational viscosity is, in fact, weakly related to the zero-shear viscosity. It characterizes stretching of polymer solution at transition from the tip of the Taylor cone to the beginning of the jet. The higher initial elongation viscosity, in fact, means a stronger stretching which might be related to a higher applied voltage. As a result of the latter the final cross-sectional fiber radius decreases at higher initial elongational viscosities as shown in Fig. 16. Although the elongational viscosity cannot be considered a fully independent input parameter, the elongational viscosity clearly represents a dominant factor in the model and in literature on strong stretching of polymeric liquids.
5. Relaxation time measures a material's ability to relax elastically from any pre-stressed state. For polymer solutions the relaxation time depends on polymer type, molecular weight, concentration, molecular structure, and the solvent type. Very limited literature data are available or reported for relaxation times of polymer solutions used in electrospinning. Refs. [18,28] provided such data. In particular, Ref. [28] provided information with regards to fiber diameter and morphology variation using an aqueous polymer solution of 32% polyethylene glycol (PEG) (MW 10,000) with a small quantity (0.10%) of varying molecular weight PEO. The solutions were considered Boger fluids, which maintain constant many material properties (i.e. zero-shear viscosity, conductivity, etc.) but have varying relaxation times (and inevitably, elongational viscosities). The data provided appeared to agree with the trend observed in the present model in that fiber's final cross-sectional radius increased with increasing relaxation time. However, the data was relatively scattered, so the comparison is still somewhat incomplete.
6. Literature sources report initial polymer concentrations ranging from 1 to 40% [18,20,21,26–30], but typically most were less than 30%. Few literature sources attempted to experimentally identify the effect of only the initial polymer concentration, while maintaining constant values for the remaining variables. Ref. [31] showed that Nylon-6 fiber diameters increase from 80 to 230 nm when increasing initial polymer concentration from 10 to 25% – the trend which agrees with the predictions in Fig. 6.
7. The model identifies the perturbation frequency as a typical frequency (10^4 Hz) of noise in a laboratory [1,2] that triggers the bending instability by introducing small initial perturbations, namely, causing some segment to move out of alignment with the rest of the jet. No literature is available on perturbation frequency as related to the electrospinning process.
8. When considering various solvents and the particular effect of vapor pressure, a true comparison may prove difficult due to the variation of other solvent properties when testing. Several studies reported on the effect of various solvents and their effect on the electrospinning process [25–27,32,33], however, most of the information is related to morphological changes due to conductivity, viscosity or surface tension. Discussion in these sources did bring up a few points related to vapor pressure (boiling point) as it relates to electrospinning of polymer solutions. First, low vapor pressure solvents tended to hasten nozzle plugging without sufficient flow to maintain a fully developed drop, due to low charge density or high viscosity. Given the lack of data on the vapor pressure effect, no worthwhile comparison to the model can be made at this time.
9. Most literature did not report solution density, but for those that did [18,26,34], the values were very close to pure solvent (within 5%). No literature was found that specifically addressed the effects of solution density on

electrospun jets' radius. Moreover, this parameter could hardly be imagined to vary alone, since solvent change inevitably affects many other physical properties, and in particular, solvent quality. For a given polymer (even being soluble in a new solvent), this will lead to a dramatic change in the rheological properties of the solution, namely in its relaxation time and elongational viscosity.

10. Ref. [19] reported an initial decrease in diameter of poly(lactide-*co*-glycolide) (PLAGA) fibers from 900 to 450 nm with an increase in electric potential from 8 to 10 kV (electric field strength of 0.4–0.5 kV/cm), but no significant correlation with subsequent increases. Polymer solution flow rate was not controlled. Ref. [35] showed that for different applied voltages (10, 15 and 20 kV), poly(acrylonitrile) (PAN) fibers developed no significant change in fiber diameter for solutions (DMF solvent) with initial polymer concentrations of 6, 8, 10 and 12%.
11. No literature research reported on vapor diffusivity effects on jet behavior or radius, so no definitive comparison with experimental data can be made on its importance. In general, vapor diffusivities in air of most of the typical solvents used in electrospinning do not differ too much, and different solvents lead to different fiber diameters (holding the other parameters constant) primarily because of their different evaporation rates. The lower evaporating solvent allowing for longer stretching process before jet solidification taking place, and thus for thinner fibers.
12. Ref. [36] described the effect of humidity on fibers, but it dealt with the development of porous fibers when electrospinning under elevated humidity. No definitive comparisons with experimental data can be currently made. The effects of relative humidity are strongly coupled to other parameters and operating conditions. This parameter may be more important through the coupled effects than this current analysis indicates.
13. Initially for surface tension, cases depicted in Fig. 13 were run based on values reported in literature for various solvents. When no noticeable change occurred in the jet radius, smaller and significantly larger values were used, even though they were outside of physical likelihood. The results show that the effect of the surface tension is negligibly small when electrospun solutions retain their viscoelasticity and experience solidification. This indeed happens in reality for most properly chosen electrospun solutions, where the viscoelastic forces completely dominate the surface tension. When low molecular weight polymers are used or polymer concentrations are significantly reduced, viscoelastic forces dramatically diminish and surface tension plays a strong role in the morphology of the resulting fibers. In such cases beaded fibers tend to form for higher surface tension solvents like water, low viscosity and low conductivity/charge density systems. Stretching is known to be a stabilizing factor in the case of capillary instability. Reduction of the volumetric charge density suppresses electrically-driven stretching and thus increases tendency toward capillary instability and bead formation.

The model results in Table 3 indicate five parameters that have a strong influence on the final diameter of the electrospinning jet, five parameters that have a moderate effect, and three parameters that have minor effect on the fiber diameter. The literature survey shows that in most cases the data reported are insufficient for direct comparison with the model results. The electrospinning process is complex and it is difficult (or in some cases, impossible) to experimentally vary one parameter while others are kept constant. Nevertheless, more careful experiments are needed to validate the model. The evaluation of the model reported here by varying one parameter at a time gives insight into the electrospinning process and suggests that to better control the process one must control the five parameters having the strongest effect. In many ways this is an oversimplification because it ignores couplings between parameters for real materials. Such couplings should be investigated in future work.

The intent of this work was to determine how strongly each parameter affects the final cross-sectional jet/fiber diameter, which was accomplished. This work does not attempt to validate the model with experimental data (which are quite incomplete).

3. Conclusions

Thirteen parameters in the electrospinning model [1,2] were varied one at a time to determine their effect on final jet cross-sectional radius. The results show that such parameters as volumetric charge density, distance from nozzle to collector, initial jet radius, relaxation time, and elongational viscosity have the largest influence on the resulting electrospun fiber diameter. Five other parameters have a moderate effect and three parameters have minor effect. These results may help guide future experiments by focusing efforts on the most important parameters. Available experimental data are insufficient to fully validate the model results for most of the parameters.

Acknowledgements

This work was supported by the Coalescence Filtration Nanomaterials Consortium: Ahlstrom Paper Group, Donaldson Company, Cummins Filtration, Hollingsworth and Vose, and Parker Hannifin. This work is also supported by the National Science Foundation grant number DMI-0403835. ALY gratefully acknowledges partial financial support by the National Science Foundation through grant NIRT CTS-0609062.

References

[1] Reneker DH, Yarin AL, Fong H, Koombhongse S. Bending instability of electrically charged liquid jets of polymer solution in electrospinning. Journal of Applied Physics 2000;87:4531–47.
[2] Yarin AL, Koombhongse S, Reneker DH. Taylor cone and jetting from liquid droplets in electrospinning of nanofibers. Journal of Applied Physics 2001;90:4836–46.
[3] Thompson C. An analysis of variable effects on a theoretical model of the electrospin process for making nanofibers, thesis. Akron, Ohio: The University of Akron; 2006.

[4] Grafe T, Graham K. Polymeric nanofibers and nanofiber webs: a new class of nonwovens. Donaldson Co., Inc. presented at INTC 2002: International Nonwovens Technical Conference; 2002. p. 1–13.
[5] Yarin AL, Zussman E. Upward needleless electrospinning of multiple nanofibers. Polymer 2004;45:2977–80.
[6] Theron A, Zussman E, Yarin AL. Electrostatic field-assisted alignment of electrospun nanofibers. Nanotechnology 2001;12:384–90.
[7] Zussman E, Theron A, Yarin AL. Formation of nanofiber crossbars in electro-spinning. Applied Physics Letters 2003;82:973–5.
[8] Reneker DH, Yarin AL, Zussman E, Xu H. Electrospinning of nanofibers from polymer solutions and melts. Advances in Applied Mechanics 2007;41:43–195.
[9] Theron SA, Yarin AL, Zussman E, Kroll E. Multiple jets in electrospinning: experiment and modeling. Polymer 2005;46:2889–99.
[10] Fridrikh SV, Yu JH, Brenner MP, Rutledge GC. Controlling the fiber diameter during electrospinning. Physical Review Letters 2003;90: 144502.
[11] Spivak AF, Dzenis YA. Asymptotic decay of radius of a weakly conductive viscous jet in an external electric field. Applied Physics Letters 1998;73:3067–9.
[12] Hohman MM, Shin M, Rutledge G, Brenner MP. Electrospinning and electrically forced jets. I. Stability theory. Physics of Fluids 2001; 13:2201–20.
[13] Hohman MM, Shin M, Rutledge G, Brenner MP. Electrospinning and electrically forced jets. II. Applications. Physics of Fluids 2001;13: 2221–36.
[14] Feng JJ. Stretching of a straight electrically charged viscoelastic jet. Journal of Non-Newtonian Fluid Mechanics 2003;116:55–70.
[15] Kowalewski TA, Blonski S, Barral S. Experiments and modeling of electrospinning process. Bulletin of the Polish Academy of Sciences 2005;53:385–94.
[16] Reznik SN, Yarin AL, Theron A, Zussman E. Transient and steady shapes of droplets attached to a surface in strong electric fields. Journal of Fluid Mechanics 2004;516:349–77.
[17] Reznik SN, Yarin AL, Zussman E, Bercovici L. Evolution of a compound droplet attached to a core-shell nozzle under the action of a strong electric field. Physics of Fluids 2006;18:062101.
[18] Theron S, Zussman E, Yarin AL. Experimental investigation of the governing parameters in the electrospinning of polymer solutions. Polymer 2004;45:2017–30.
[19] Katti DS, Robinson KW, Ko FK, Laurencin CT. Bioresorbable nanofiber-based systems for wound healing and drug delivery: optimization of fabrication parameters. Journal of Biomedical Materials Research 2004; 70B:286–96.
[20] Fong H, Chun I, Reneker DH. Beaded nanofibers formed during electrospinning. Polymer 1999;40:4585–92.
[21] Zuo W, Zhu M, Yang W, Yu H, Chen Y, Zhang Y. Experimental study on relationship between jet instability and formation of beaded fibers during electrospinning. Polymer Engineering and Science 2005;45:704–9.
[22] Doshi J, Reneker DH. Electrospinning process and applications of electrospun fibers. Journal of Electrostatics 1995;35:151–60.
[23] Supaphol P, Mit-Uppatham C, Nithitanakul M. Ultrafine electrospun polyamide-6 fibers: effect of emitting electrode polarity on morphology and average fiber diameter. Journal of Polymer Science Part B: Polymer Physics 2005;43:3699–712.
[24] Mit-Uppatham C, Nithitanakul M, Supaphol P. Effects of solution concentration, emitting electrode polarity, solvent type, and salt addition on electrospun polyamide-6 fibers: a preliminary report. Macromolecular Symposia 2004;216:293–9.
[25] Wannatong L, Sirivat A, Supaphol P. Effects of solvents on electrospun polymeric fibers: preliminary study on polystyrene. Polymer International 2004;53:1851–9.
[26] Jarusuwannapoom T, Hongrojjanawiwat W, Jitjaicham S, Wannatong L, Nithitanakul M, Pattamaprom C, et al. Effect of solvents on electrospinnability of polystyrene solutions and morphological appearance of resulting electrospun polystyrene fibers. European Polymer Journal 2005;41:409–21.
[27] Arayanarakul K, Choktaweesap N, Aht-Ong D, Meechaisue C, Supaphol P. Effects of poly(ethylene glycol), inorganic salt, sodium dodecyl sulfate, and solvent system on electrospinning of poly(ethylene oxide). Macromolecular Materials and Engineering 2006;291:581–91.
[28] Yu JH, Fridrikh SV, Rutledge GC. The role of elasticity in the formation of electrospun fibers. Polymer 2006;47:4789–97.
[29] Deitzel JM, Kleinmeyer JD, Harris D, Beck Tan NC. The effect of processing variables on the morphology of electrospun nanofibers and textiles. Polymer 2001;42:261–72.
[30] Son WK, Youk JH, Lee TS, Park WH. The effects of solution properties and polyelectrolyte on electrospinning of ultrafine poly(ethylene oxide) fibers. Polymer 2004;45:2959–66.
[31] Chase GG, Reneker DH. Nanofibers in filter media. Fluid/Particle Separation Journal 2004;16:105–17.
[32] Yang Q, Li Z, Hong Y, Zhao Y, Qiu S, Wang C, et al. Influence of solvents on the formation of ultrathin uniform poly(vinyl pyrrolidone) nanofibers with electrospinning. Journal of Polymer Science Part B: Polymer Physics 2004;42:3721–6.
[33] Gupta P, Elkins C, Long TE, Wilkes GL. Electrospinning of linear homopolymers of poly(methyl methacrylate): exploring relationships between fiber formation, viscosity, molecular weight and concentration in a good solvent. Polymer 2005;46:4799–810.
[34] Samatham R, Kim KJ. Electric current as a control variable in the electrospinning process. Polymer Engineering and Science 2006;46:954–9.
[35] Gu SY, Ren J, Vancso GJ. Process optimization and empirical modeling for electrospun polyacrylonitrile (PAN) nanofiber precursor of carbon nanofibers. European Polymer Journal 2005;41:2559–68.
[36] Casper CL, Stephens JS, Tassi NG, Chase DB, Rabolt JF. Controlling surface morphology of electrospun polystyrene fibers: effect of humidity and molecular weight in electrospinning process. Macromolecules 2004;37:573–8.